Modeling of a New ZVS Bi-directional DC-DC Converter

HUI LI
Florida State University

FANG Z. PENG
Michigan State University

A dual half-bridge (DHB) bidirectional dc-dc converter is a new proposed topology that has the advantages of decreased number of devices, soft-switching implementation, low cost, and high efficiency. Typical applications of this converter are the auxiliary power supply in fuel cell vehicles and battery charging and discharging systems where the power density, cost, weight, and reliability are critical factors. A switching-frequency-dependent state-space averaged model of the converter is developed here for either direction of power flow. This averaged model can be used to derive the steady-state characteristics and small signal dynamics of the proposed topology. It also provides a fast simulation tool to investigate the transient response of the converter. The simulated waveforms of the mathematical model are compared with the detailed circuit simulation to verify the accuracy of the modeling.

Manuscript received March 3, 2003; revised October 6, 2003; released for publication November 25, 2003.

IEEE Log No. T-AES/40/1/826474.

Refereeing of this contribution was handled by William M. Polivka.

Authors' addresses: H. Li, Florida A&M University–Florida State University, College of Engineering, Dept. of Electrical & Computer Engineering, 2525 Pottsdamer St., Tallahassee, FL 32310-6046, E-mail: (hil@caps.fsu.edu); F. Z. Peng, Dept. of Electrical & Computer Engineering, Michigan State University, East Lansing, MI 48824.

I. INTRODUCTION

Fuel cell technology is a prospective candidate to replace the widely used internal combustion engines in traditional cars or conventional batteries used in today's electric vehicles and to become the primary power source for the next generation hybrid electric vehicles. Because of the lack of an energy storage function in the fuel cell, it is required to have a relatively large dc-dc converter for an auxiliary energy storage application. Fig. 1 is a block diagram of the fuel cell power bus and energy management system in a hybrid electrical vehicle. The battery voltage is usually selected as 12 V for compatibility with the majority of today's automobile loads. The system operation is to have the 12 V battery derived power to boost the high voltage bus up to 288 V during starting. Then this voltage is provided for the fuel cell compressor motor expanding unit controller and to bring up the fuel cell voltage, which in turn feeds back to the high voltage bus to release the loading from the battery. In addition, regenerated power from the traction motor is absorbed by the battery.

For such a fuel-cell energy system application, the functions of this dc-dc converter are two-fold: first, to boost the high voltage bus to a desired voltage before the fuel cell can generate power; and second, to store the regenerative power from the traction motor drive. Full bridge bidirectional dc-dc converters with soft-switching [1–4] are considered a suitable choice for the above application because of their capabilities to handle bidirectional high power and reduce switching loss. Recently, a new soft-switched isolated bidirectional dc-dc with dual half-bridge (DHB) was introduced in [5]. Compared to full bridge counterparts, it has half the component count for the same power rating with no total-device-rating penalty. In addition, unified zero-voltage-switching (ZVS) is achieved in either direction of power flow without any additional components. Therefore, a minimum number of devices are required in the circuit. Also the design has less control and accessory power. All these new features allow efficient power conversion, easy control, lightweight and compacted packaging. However, the advantages of the proposed DHB converter are obtained at the expense of increasing the order of the system. Therefore there is a need to study the dynamics of this high order system.

In the literature, the research on the soft-switching full bridge bidirectional dc-dc converters has been restricted to circuit topologies and steady-state analysis [1–4]. Although circuit simulation based on Pspice-like software can offer cycle-by-cycle performance, it is inconvenient and time-consuming to study the long-term dynamic behavior such as the start-up performance. Nor can it provide information of poles, zeros, and the gain of the converter around the operating point to design the controller. The goal of the work presented here is

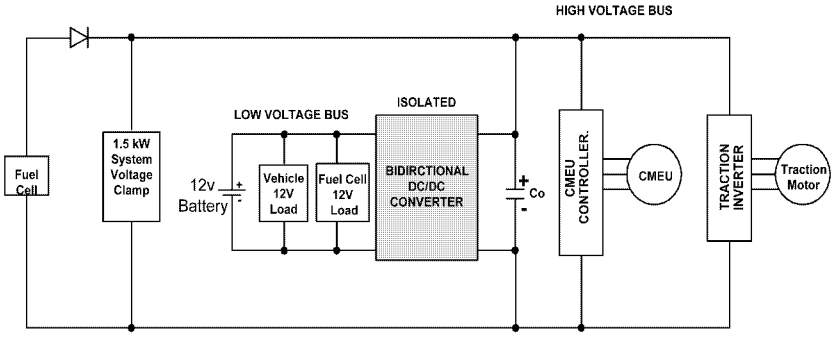

Fig. 1. Block diagram of fuel cell power bus and energy management system.

to develop the mathematical model for the proposed DHB bidirectional dc-dc converter to study the dynamics and design the controller. In Section II, the basic operation principles of DHB are described briefly to help understand the large-signal operation of the converter. The detailed description of the circuit can be found in [5]. Section III concentrates on the derivation of a generalized state-space model for either direction of power flow by using averaging method similar to "alternor concept" [9–10]. A simulation model based on averaged model is also presented. The simulated waveforms of open-loop system are compared with the detailed circuit simulation to verify the accuracy of the modeling. A 1.6 kW prototype has been built. The output characteristics have been measured and compared with simulation results to verify the averaged model further. In Section IV the steady-state characteristics are derived from the averaged model and proved to be consistent with that derived from circuit analysis of Section II. In addition, a small signal model is developed and the transfer functions of the converter are presented in Section VI. A controller is designed to make the system have satisfactory dynamic performance for fuel cell applications.

II. CONVERTER DESCRIPTION

Fig. 2 illustrates the DHB converter topology and the commutation waveforms in boost mode. ZVS is achieved by operating the two half-bridges with a phase shift. This operation allows a resonant discharge of the lossless snubber capacitances of the switching devices and each device's antiparallel diode is conducted before the conduction of switching devices.

Since the operation has been described in detail in [5], we only emphasize the circuit operation that is significant for the development of the averaged model. Fig. 3 is the primary-referred equivalent circuit. The current i_r and voltages v_3, v_4 are the primary-referred transformer current and capacitor voltages. All the switches are considered to have instantaneous turn-on and turn-off. The circuit operation uses the transformer leakage inductance as an interface and energy transfer element between the two voltage-source half bridge converters: low voltage side (LVS) and high voltage side (HVS) half-bridges, so replacing the transformer with a leakage inductance L_s in Fig. 2 simplifies circuit analysis. R_b and R_s can be regarded as collective resistance of the inner resistance of voltage sources/or load resistances, inductor resistance, transformer resistance, and switch-loss equivalent resistances of LVS and HVS. Fig. 4 presents the voltage and current waveforms of the transformer during one switching period. The circuit is operated with dual active half-bridge, which can be shown from Fig. 4. In fuel cell applications, when power flows from the LVS to the HVS, the circuit works in boost mode to keep the HVS voltage at a desired high value before fuel cell can generate power. In the other direction of power flow, the circuit works in buck mode to absorb regenerated energy. Based on the idealized waveforms in Fig. 4, there are four operation modes in one switching cycle, and the transformer current i_r of each mode can be calculated as follows:

$$\begin{cases} \text{Mode I:} & i_r = (v_1 + v_4)\theta/\omega L_s + i_r(0) \\ \text{Mode II:} & i_r = (v_1 - v_3)(\theta - \phi_1)/\omega L_s + i_r(\phi_1) \\ \text{Mode III:} & i_r = (-v_2 - v_3)(\theta - \pi)/\omega L_s + i_r(\pi) \\ \text{Mode IV:} & i_r = (-v_2 + v_4)(\theta - \pi - \phi_1)/\omega L_s + i_r(\pi + \phi_1) \end{cases} \tag{1}$$

The current initial conditions can be solved using the boundary conditions of

$$i_r(0) = -i_r(\pi)$$

$$i_r(\phi_1) = -i_r(\pi + \phi_1).$$

The initial conditions of i_r are solved in (2)

$$\begin{cases} i_r(0) = \dfrac{v_3 - v_1}{2\omega L_S}(\pi - \phi_1) - \dfrac{v_1 + v_4}{2\omega L_S}\phi_1 \\ i_r(\phi_1) = \dfrac{v_1 + v_4}{2\omega L_S}\phi_1 + \dfrac{v_3 - v_1}{2\omega L_S}(\pi - \phi_1) \\ i_r(\pi) = -i_r(0) \\ i_r(\pi + \phi_1) = -i_r(\phi_1). \end{cases} \tag{2}$$

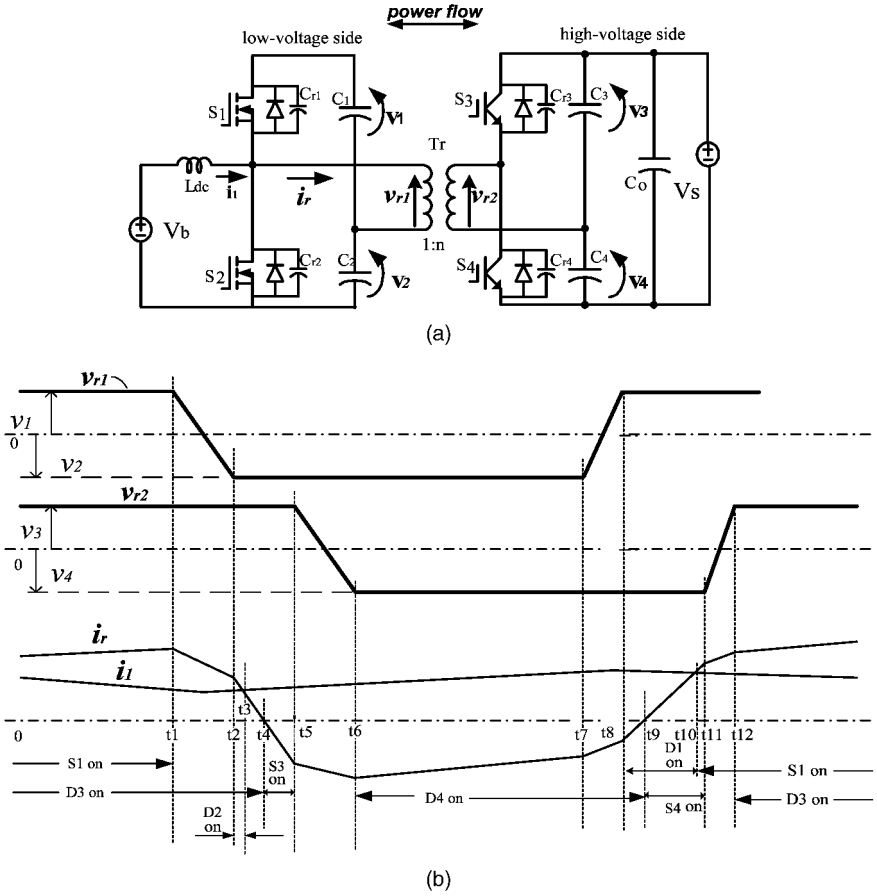

Fig. 2. Soft-switched bidirectional half-bridge dc-dc converter. (a) DHB converter topology. (b) Commutation waveforms and switching timing of DHB converter in boost mode.

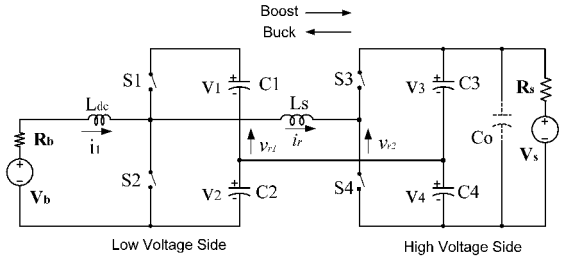

Fig. 3. Primary-referred equivalent circuits.

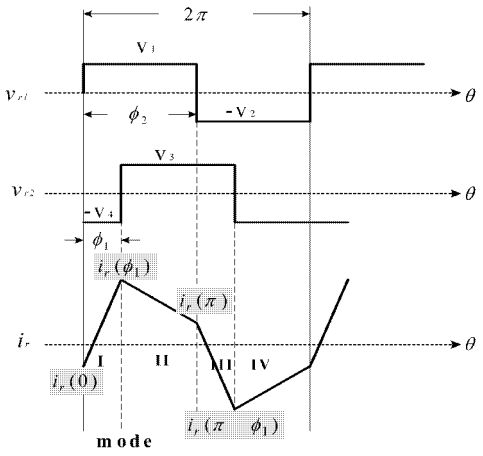

Fig. 4. Idealized voltage and current waveforms of transformer.

Further, the output power can be found to be

$$P_o = \frac{\int_0^{T_S} i_r \cdot v_{r1} dt}{T_s} = \frac{\phi_1 \frac{1}{D}\left[4\pi(1-D) - \frac{1}{D}\phi_1\right]}{4\pi\omega L_S} \cdot V_{\text{in}}^2. \tag{3}$$

T_s is the period of the switching frequency, V_{in} is the V_b in boost mode and V_s in buck mode, and $D = \phi_2/2\pi$. The output power (output voltage) can be regulated by phase shift angle ϕ_1, duty cycle D, and switching frequency ω. If $D = 50\%$ is assumed, then the output power equation can be simplified further as

$$P_o = \frac{V_{\text{in}}^2}{\omega L_s} \frac{\phi_1(\pi - \phi_1)}{\pi}. \tag{4}$$

Because of the symmetric property of dual active half-bridges, the operation principles of boost mode and buck mode are the same except the polarity of phase shift angle, which can also be shown in Fig. 4. Therefore a generalized averaged model is possible to be developed for both modes.

III. STATE-SPACE MATHEMATICAL MODEL DEVELOPMENT AND VERIFICATION

A. Mathematical Model Derivation

The state variables of the proposed converter are chosen to be the inductor current i_1, transformer current i_r, and the capacitor voltages v_1, v_2, v_3, and v_4, which are defined in the circuit of Fig. 3. It is noted from Fig. 4 that state variables v_1, v_2, v_3, and v_4 vary slowly with time, also does i_1 if enough large inductance is selected, while the state variable i_r varies quickly with time. The dynamical system thereby consists of a fast variable and a slow subsystem. By applying the averaging method, the slow subsystem can be dealt with as a time-invariant (dc) nonlinear model.

To analyze the behavior of the fast variable i_r, the other slow state variables can be treated as dc constants. From a system point of view, only the average of the fast state variable has effects on the slow state variables. Therefore, the averaging model of the slow subsystem is obtained by substituting the fast variables by their moving average into the slow subsystem. The similar idea has also been described in [7–10].

From Section II, we know that the converter is operated as dual active half-bridges and there are four operation modes during one switching cycle. Therefore two switch functions S_p and S_s are introduced in Fig. 5, which corresponds to the gate signal of LVS switches and HVS devices, respectively.

With the help of switching functions, the state equation of the slow state variables is described by

$$\begin{aligned}
\dot{i}_1 &= [v_b - i_1 R_b - S_p(v_1 + v_2)]/L_{\mathrm{dc}} \\
\dot{v}_1 &= -S_p i_r/C_p + S_p i_1/C_p \\
\dot{v}_2 &= i_r(1 - S_p)/C_p + S_p i_1/C_p \\
\dot{v}_3 &= [-(v_3 + v_4 - v_s)/R_s - C_o d(v_3 + v_4)/dt](1 - S_s)/C_s \\
&\quad + [i_r - (v_3 + v_4 - v_s)/R_s - C_o \cdot d(v_3 + v_4)/dt]S_s/C_s \\
\dot{v}_4 &= [(-i_r + (v_3 + v_4 - v_s)/R_s - C_o \cdot d(v_3 + v_4)/dt)] \cdot (1 - S_s)/C_s \\
&\quad + [-(v_3 + v_4 - v_s)/R_s - C_o \cdot d(v_3 + v_4)/dt]S_s/C_s
\end{aligned} \tag{5}$$

where $C_p = C_1 = C_2$, and $C_s = C_3 = C_4$.

This equation describes all the operation modes of one switching cycle in Fig. 4. The next step is to calculate the integration of fast variable i_r in $[0, \phi_1]$, $[\phi_1, \pi]$, $[\pi, \pi + \phi_1]$, $[\pi + \phi_1, 2\pi]$, respectively based on (1) and (2). Then substitute the above results and switch functions S_p and S_s into (5) to calculate the moving averages of the slow variables shown in (6),

$$\begin{aligned}
i_{1\,\mathrm{avg}} &= \frac{\int_t^{t+T_s} i_1 dt}{T_s}, \qquad v_{1\,\mathrm{avg}} = \frac{\int_t^{t+T_s} v_1 dt}{T_s} \\
v_{2\,\mathrm{avg}} &= \frac{\int_t^{t+T_s} v_2 dt}{T_s}, \qquad v_{3\,\mathrm{avg}} = \frac{\int_t^{t+T_s} v_3 dt}{T_s} \\
v_{4\,\mathrm{avg}} &= \frac{\int_t^{t+T_s} v_4 dt}{T_s}.
\end{aligned} \tag{6}$$

The state-space averaged model of DHB converter is derived as follows:

$$\begin{bmatrix} \dot{i}_{1\,\mathrm{avg}} \\ \dot{v}_{1\,\mathrm{avg}} \\ \dot{v}_{2\,\mathrm{avg}} \\ \dot{v}_{3\,\mathrm{avg}} \\ \dot{v}_{4\,\mathrm{avg}} \end{bmatrix} = \begin{bmatrix} -\frac{R_b}{L_{\mathrm{dc}}} & -\frac{1}{2L_{\mathrm{dc}}} & -\frac{1}{2L_{\mathrm{dc}}} & 0 & 0 \\ \frac{1}{2C_p} & 0 & 0 & \frac{-\phi_1(\pi-\phi_1)}{\mathrm{con}\,1} & \frac{-\phi_1(\pi-\phi_1)}{\mathrm{con}\,1} \\ \frac{1}{2C_p} & \frac{\phi_1^2 + (\pi-\phi_1)^2}{\mathrm{con}\,1} & \frac{-\phi_1^2 - (\pi-\phi_1)^2}{\mathrm{con}\,1} & \frac{-[\phi_1^2 + \phi_1(\pi-\phi_1) + (\pi-\phi_1)^2]}{\mathrm{con}\,1} & \frac{\phi_1^2 - \phi_1(\pi-\phi_1) + (\pi-\phi_1)^2}{\mathrm{con}\,1} \\ 0 & \left(\begin{array}{c}\frac{\phi_1^2 + 2\phi_1(\pi-\phi_1)}{\mathrm{con}\,2} \\ +\frac{[\phi_1^2 + (\pi-\phi_1)^2]C_o}{\mathrm{con}\,3}\end{array}\right) & \left(\begin{array}{c}-\frac{\phi_1^2}{\mathrm{con}\,2} \\ -\frac{[\phi_1^2 + (\pi-\phi_1)^2]C_o}{\mathrm{con}\,3}\end{array}\right) & \left(\begin{array}{c}\frac{-[\phi_1^2 + \phi_1(\pi-\phi_1)]}{\mathrm{con}\,2} \\ -\frac{[\phi_1^2 + (\pi-\phi_1)^2]C_o}{\mathrm{con}\,3} - \frac{1}{C_t R_s}\end{array}\right) & \left(\begin{array}{c}\frac{\phi_1^2 + \phi_1(\pi-\phi_1)}{\mathrm{con}\,2} \\ +\frac{[\phi_1^2 + (\pi-\phi_1)^2]C_o}{\mathrm{con}\,3} - \frac{1}{C_t R_s}\end{array}\right) \\ 0 & \left(\begin{array}{c}\frac{(\phi_1-\pi)(\pi-3\phi_1)}{\mathrm{con}\,2} \\ -\frac{[\phi_1^2 + (\pi-\phi_1)^2]C_o}{\mathrm{con}\,3}\end{array}\right) & \left(\begin{array}{c}\frac{(\pi-\phi_1)^2}{\mathrm{con}\,2} \\ +\frac{[\phi_1^2 + (\pi-\phi_1)^2]C_o}{\mathrm{con}\,3}\end{array}\right) & \left(\begin{array}{c}\frac{(\phi_1-\pi)(2\phi_1-\pi)}{\mathrm{con}\,2} \\ +\frac{[\phi_1^2 + (\pi-\phi_1)^2]C_o}{\mathrm{con}\,3} - \frac{1}{C_t R_s}\end{array}\right) & \left(\begin{array}{c}\frac{-(\phi_1-\pi)(2\phi_1-\pi)}{\mathrm{con}\,2} \\ -\frac{[\phi_1^2 + (\pi-\phi_1)^2]C_o}{\mathrm{con}\,3} - \frac{1}{C_t R_s}\end{array}\right) \end{bmatrix} \begin{bmatrix} i_{1\,\mathrm{avg}} \\ v_{1\,\mathrm{avg}} \\ v_{2\,\mathrm{avg}} \\ v_{3\,\mathrm{avg}} \\ v_{4\,\mathrm{avg}} \end{bmatrix} + \begin{bmatrix} \frac{1}{Ldc} & 0 \\ 0 & 0 \\ 0 & 0 \\ 0 & \frac{1}{C_t R_s} \\ 0 & \frac{1}{C_t R_s} \end{bmatrix} \begin{bmatrix} v_b \\ v_s \end{bmatrix} \tag{7}$$

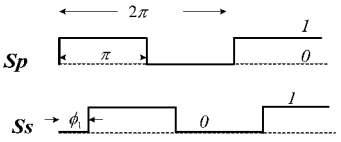

Fig. 5. Waveforms of switch function S_p and S_s.

where $\text{con}1 = C_P T_s\omega \cdot 2\omega L_s$, $\text{con}2 = C_t T_s\omega \cdot 2\omega L_s$, $\text{con}3 = C_t C_s T_s\omega \cdot 2\omega L_S$, and $C_t = C_s + 2C_o$.

According to the circuit analysis, $v_1 = v_2$ and $v_3 = v_4$ exist when $D = 50\%$. Equation (7) can be further simplified as a third-order state equation in (8) if $D = 50\%$

$$\begin{cases} \dot{i}_{1\text{avg}} = -\dfrac{R_b}{L_{\text{dc}}} i_{1\text{avg}} - \dfrac{1}{2L_{\text{dc}}} v_{12\text{avg}} + \dfrac{1}{L_{\text{dc}}} v_b \\ \dot{v}_{12\text{avg}} = \dfrac{1}{C_p} i_{1\text{avg}} - \dfrac{2\phi_1(\pi - \phi_1)}{C_p T_s\omega \cdot 2\omega L_s} v_{34\text{avg}} \\ \dot{v}_{34\text{avg}} = \dfrac{2\phi_1(\pi - \phi_1)}{C_t T_s\omega \cdot 2\omega L_s} v_{12\text{avg}} - \dfrac{2}{C_t R_s} v_{34\text{avg}} + \dfrac{2}{C_t R_s} v_s \end{cases} \tag{8}$$

where $v_{12\text{avg}} = v_{1\text{avg}} + v_{2\text{avg}}$, and $v_{34\text{avg}} = v_{3\text{avg}} + v_{4\text{avg}}$. This is a generalized averaged model for either direction of power flow. In boost mode, for example, $v_s = 0$, R_s is the load resistance, R_b can be zero or a small inner resistance of v_b, and phase shift angle ϕ_1 is positive. In buck mode, $v_b = 0$, R_b is the load resistance, R_s can be zero or a small inner resistance of v_s, and phase shift angle ϕ_1 is negative.

The averaged model can provide not only the information of slow state variables but that of fast variable i_r as well. The envelopes of the ac current i_r in one switching cycle, which is shown in Fig. 4, can be solved based on averaged model and (4).

B. Model Verification by Simulation Results

Since the state-space averaged model describes the averaged behavior of the system and the detailed circuit model presents the instantaneous performance, the developed mathematical model can be verified by comparing the simulation results with the averaged values of those from detailed circuit model [11]. A simulation block diagram of the converter based on averaged mathematical model using Matlab/Simulink is developed in Fig. 6. The detailed circuit model is built using PSIM, a Pspice-like software. In the following, a dynamic response of converter in boost mode and buck mode is simulated, respectively, and compared with those with detailed circuit simulation to verify the model in both modes.

1) *Boost Mode*: A start-up process of the open-loop converter system using a ramp input voltage of 12 V is simulated under these conditions: $V_b = 12$ V, $R_b = 0$ ohm, $D = 50\%$, $f_s = 20$ kHz, $L_{\text{dc}} = 5$ μH, $L_s = 0.30$ μH, $C_p = C_s = 10$ mF, $C_o = 169$ mF, $V_s = 0$ V, and $R_s = 0.27$ Ω.

These parameters are selected according to a 1.6 kW converter for fuel cell application. The waveforms for i_1, $v_{12}(v_1 + v_2)$, and $v_{34}(v_3 + v_4)$ of the average model and detailed circuit model are shown in Fig. 7 and Fig. 8, respectively, where v_{34} are the primary-referred output voltages. The simulation and verification of the fast variable is demonstrated in Fig. 9. The comparison demonstrates their similarity consistence in shape, frequency, and average magnitude. The simulation time is significantly decreased by using averaged simulation model, which is another advantage of applying mathematical model instead of using circuit model to simulate the converter performance.

2) *Buck Mode*: Similarly, the dynamic process of buck mode can also be simulated using this average model. The simulation results are demonstrated and compared with detailed circuit simulation in Figs. 10–12, where V_o in this case is the voltage across resistor R_b. The simulation conditions are defined as follows. $V_b = 0$ V, $R_b = 0.09$ Ω, $D = 50\%$, $f_s = 20$ kHz, $L_{\text{dc}} = 5$ μH, $L_s = 0.5625$ μH, $C_p = C_s = 10$ mF, $C_o = 0$ mF, $V_= 12$ V, and $R_s = 1$ Ω.

C. Model Verification by Experimental Results

A 1.6 kW soft-switched bidirectional dc-dc converter has been built and experimentally tested

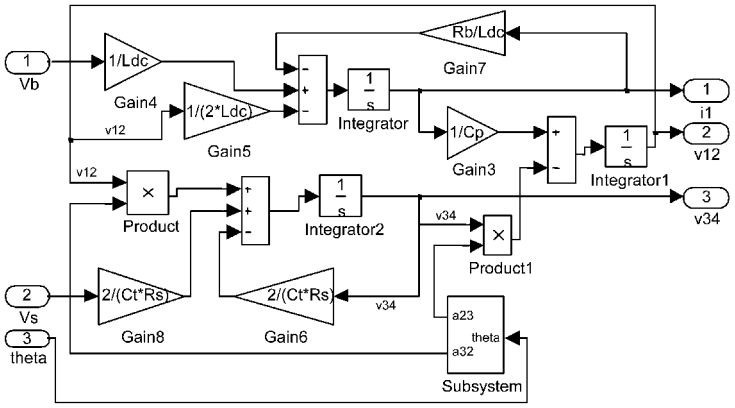

Fig. 6. Simulation block diagram of average mode using Matlab/Simulink.

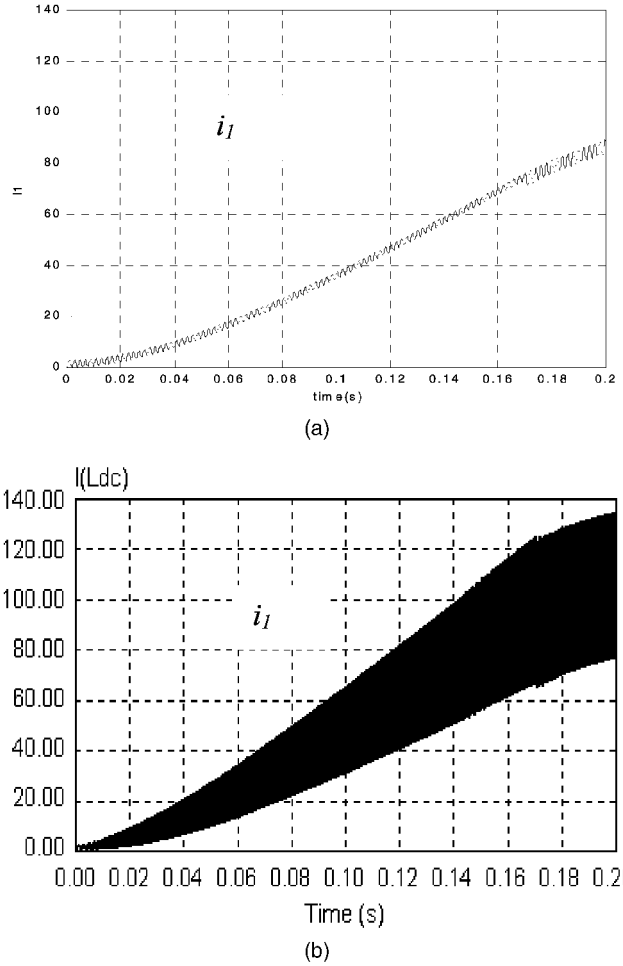

Fig. 7. Simulation and comparison of i_1 in boost. (a) i_1 of average model. (b) i_1 of detailed circuit simulation.

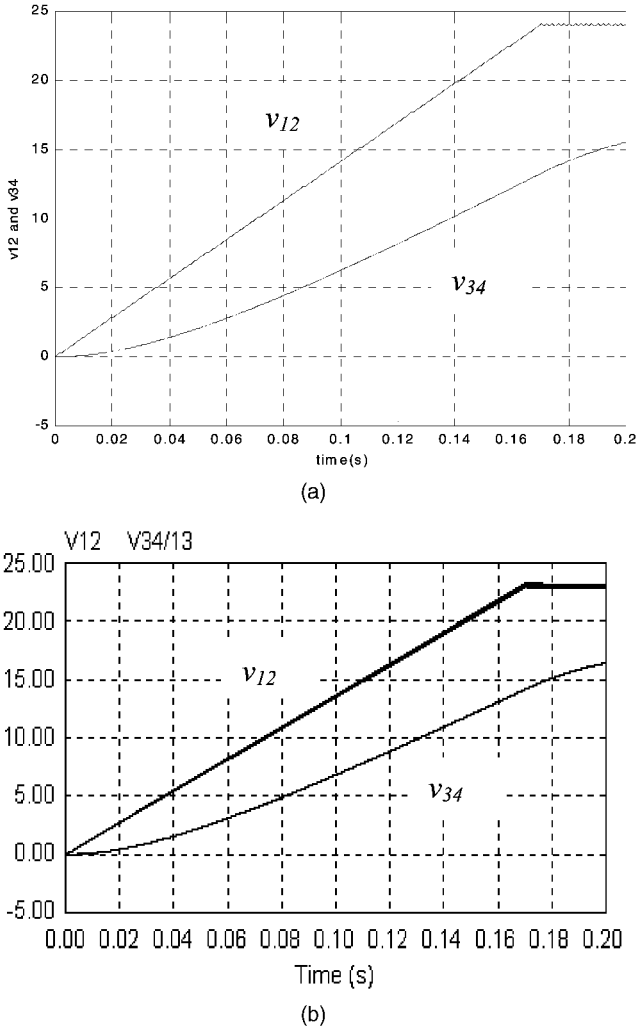

Fig. 8. Simulation and comparison of v_{12} and v_{34} in boost mode. (a) v_{12} and v_{34} of average model. (b) v_{12} and v_{34} of detailed circuit simulation.

to validate the developed model. The prototype is pictured in Fig. 13. The overall size is about 7.25″ width and 8.5″ in length. Fig. 14 presents the output characteristics of the converter from 0 to full output power under open-loop condition. As indicated in the figure, the "*" trace is the experimental result, the "o" curve is of detailed circuit simulation and the "+" one is of average model simulation. In order to compare three results, all the outputs are converted to the secondary side of the transformer in which the turns ratio is 1 : 13. The similarity of these three curves confirms the validity of the average model. The difference between the average model, detailed circuit model and prototype can be explained as follows. The average model assumes all switches and components are ideal and that there are no losses in switches, capacitors, the inductor or the transformer. PSIM software package is used to simulate the detail circuit, where the switches, capacitors, inductor, and transformer are not treated in ideal cases. The conduction loss of the switches and copper loss of other components, and etc., is brought in by defining the corresponding parameters in the device simulation models. The detailed circuit model is therefore a better approximation of the actual circuit and the efficiency will be lower than that of average model. The difference between the circuit model and the prototype is likely in the higher device losses and magnetic losses in the prototype due to the imperfect devices and transformer models in detailed circuit simulation. Thereby, the output voltage of average model is higher than that of the detailed circuit model and the detailed circuit model voltage is higher than the prototype.

IV. STEADY-STATE AND DYNAMIC ANALYSIS

The developed mathematical model can be used to study not only the dynamics such as the above converter start-up behavior, but also the steady-state features and small signal dynamics of the converter, which are shown as follows.

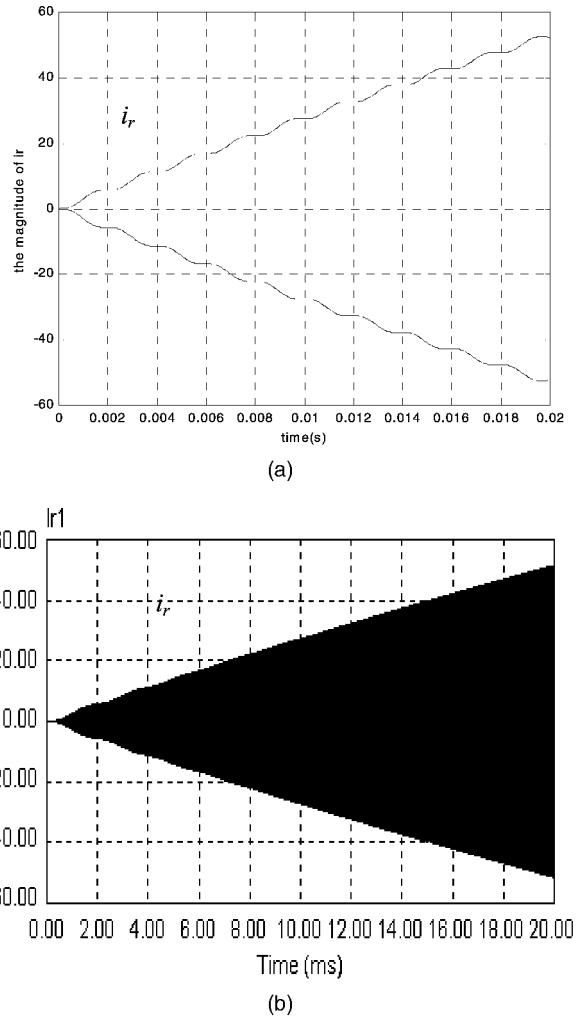

Fig. 9. Simulation and comparison of envelope of i_r in boost mode. (a) Envelope of i_r of average mode simulation. (b) Envelope of i_r of detailed circuit simulation.

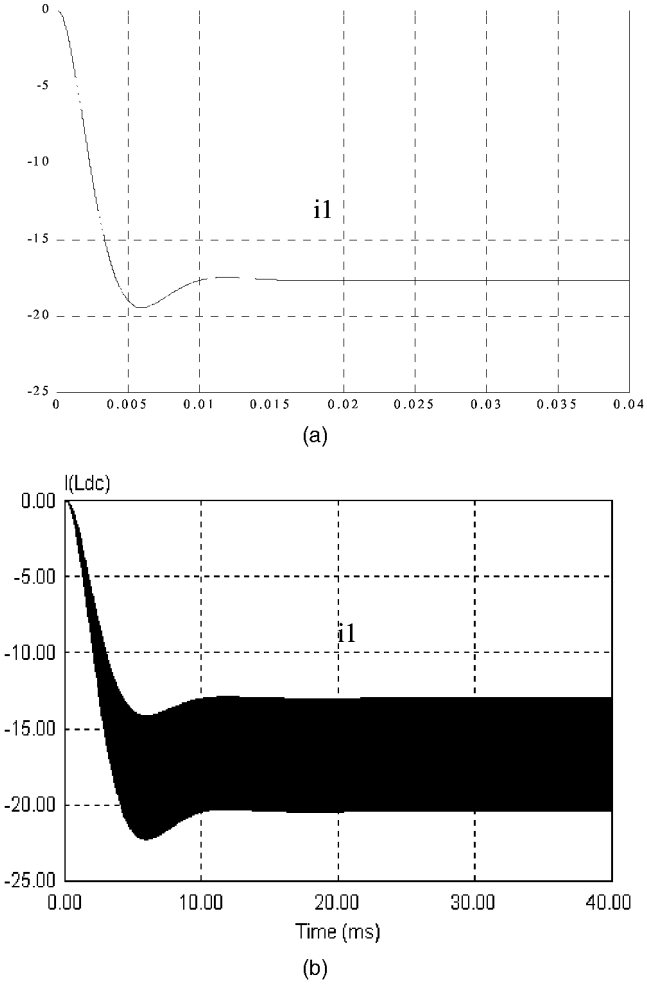

Fig. 10. Simulation and comparison of i_1 in buck mode. (a) i_1 of average model. (b) i_1 of detailed circuit simulation.

A. Steady-State Characteristics

The steady state, i.e., nominal operating point can be obtained by setting the following values in (8). $\dot{i}_1 = 0$, $\dot{v}_{12} = 0$, $\dot{v}_{34} = 0$, $i_o = 0$, $v_{\text{in}} = V_{\text{in}}$, $\phi_1 = \Phi_1$.

Using boost mode as an example and take $D = 50\%$, all the state variables at steady state are calculated as follows:

$$\begin{cases} I_1 = \dfrac{V_{\text{in}} \cdot \Phi_1^2 \cdot (\pi - \Phi_1)^2 \cdot R}{T_s^2 \cdot L_s^2 \cdot \omega^4} \\ V_{12} = 2V_{\text{in}} \\ V_{34} = \dfrac{V_{\text{in}} \cdot \Phi_1 \cdot (\pi - \Phi_1) \cdot R}{2\pi\omega L_s} \end{cases} \tag{9}$$

where Φ_1 is the steady-state phase shift. Therefore, by controlling phase shift angle and switching frequency, the output voltage is regulated. Substituting V_{in}, I_1, and V_{34} into the power equations $P_{\text{in}} = V_{\text{in}} \cdot I_1$, and $P_o = v_{34}^2/R$, it is easy to calculate the transfer power of nominal operating point as follows

$$P_{\text{in}} = P_o = \frac{V_{\text{in}}^2 \cdot \Phi_1^2 \cdot (\pi - \Phi_1)^2 \cdot R}{(2\pi\omega L_s)^2}. \tag{10}$$

Equation (10) can also be represented as

$$P_{\text{in}} = P_o = \frac{V_{\text{in}} \cdot \Phi_1 \cdot (\pi - \Phi_1) \cdot V_{34}}{2\pi\omega L_s}. \tag{11}$$

And $V_{34} = V_{12} = 2V_{\text{in}}$ when $D = 50\%$. Substituting $V_{34} = 2V_{\text{in}}$ in (11), (11) becomes the same as (4) which was derived from circuit analysis in Section II.

B. Small-Signal Model Analysis

With the generalized state-space averaged model, the small signal model of the proposed converter in boost mode and buck mode can be derived respectively. However, the small-signal dynamics of boost-type converter is more complicated than buck-type converter due to the right half plane (RHP) zero and depending on the operating point. The new DHB converter in boost mode is therefore selected

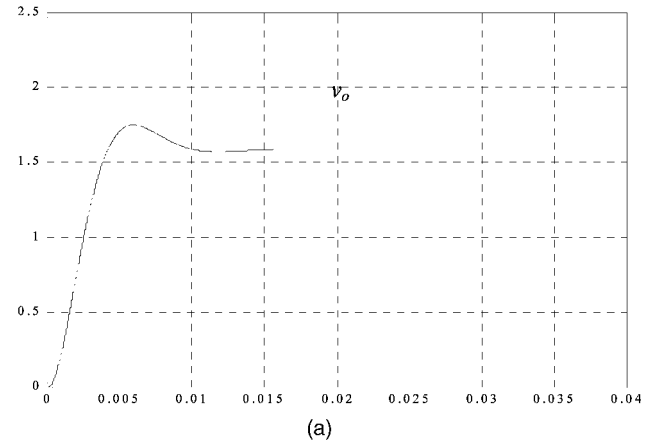

(a)

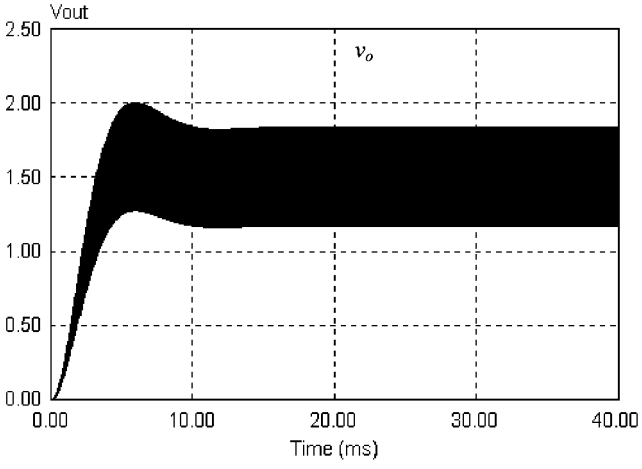

(b)

Fig. 11. Simulation and comparison of v_o in buck mode. (a) V_o of average model. (b) V_o of detailed circuit simulation.

as an example to show the derivation of small signal model and the corresponding transfer functions. The analysis in buck mode can be derived similarly.

1) *Small-Signal Model Derivation*: To account for the variation of the load, a current source $i_o = \Delta G \cdot v_o$ is placed across the nominal load conductance G as shown in Fig. 15. The averaged model, taking account of the variation in load, is then developed from (8)

$$\begin{cases} \dot{i}_1 = \dfrac{-1}{2L_{\rm dc}} v_{12} + \dfrac{1}{L_{\rm dc}} v_{\rm in} \\ \dot{v}_{12} = \dfrac{1}{C_p} i_1 - \dfrac{2\phi_1(\pi-\phi_1)}{C_p T_s \omega \cdot 2\omega L_s} v_{34} \\ \dot{v}_{34} = \dfrac{2\phi_1(\pi-\phi_1)}{(C_s+2C_o)T_s\omega \cdot 2\omega L_s} v_{12} \\ \qquad -\dfrac{2}{(C_s+2C_o)R} v_{34} - \dfrac{2}{C_s+2C_o} i_o. \end{cases} \tag{12}$$

Compared with (8), which is a unified averaged model for both boost mode and buck mode, the derivative of i_1 of (12) is missing the item "$-R_{b\bullet} i_{1\,\rm avg}/L_{\rm dc}$." This is because when the converter is operated in boost mode, R_b can be regarded as the inner resistance of the battery, which is very small and zero at ideal case. Therefore R_b can be ignored in (12) to simplify the derivation of small signal model. By introducing small perturbations around the nominal operating point as follows: $v_{\rm in} = V_{\rm in} + \tilde{v}_{\rm in}$, $\phi_1 = \Phi_1 + \tilde{\phi}_1$, $i_o = 0 + \tilde{i}_o$, $v_{12} = V_{12} + \tilde{v}_{12}$, $i_1 = I_1 + \tilde{i}_1$, $v_{34} = V_{34} + \tilde{v}_{34}$, and choosing $(\tilde{i}_1, \tilde{v}_{12}, \tilde{v}_{34})$ as state variables, $(\tilde{v}_{\rm in}, \tilde{\phi}_1, \tilde{i}_o)$ as control inputs, and $\tilde{v}_{34}$ as controlled output, and assuming that $|\tilde{v}_{\rm in}| \ll V_{\rm in}$, $|\tilde{\phi}_1| \ll \Phi_1$, $|\tilde{v}_{12}| \ll V_{12}$, $|\tilde{v}_{34}| \ll V_{34}$, $|\tilde{i}_1| \ll I_1$. The linearized small signal model can be derived as follows

$$\begin{cases} \begin{bmatrix} \dot{\tilde{i}}_1 \\ \dot{\tilde{v}}_{12} \\ \dot{\tilde{v}}_{34} \end{bmatrix} = \begin{bmatrix} 0 & -\dfrac{1}{2L_{\rm dc}} & 0 \\ \dfrac{1}{C_p} & 0 & \dfrac{-2\Phi_1(\pi-\Phi_1)}{\rm con\,1} \\ 0 & \dfrac{2\Phi_1(\pi-\Phi_1)}{\rm con\,3} & \dfrac{-2}{C_t R} \end{bmatrix} \begin{bmatrix} \tilde{i}_1 \\ \tilde{v}_{12} \\ \tilde{v}_{34} \end{bmatrix} \\ \qquad + \begin{bmatrix} \dfrac{1}{Ldc} & 0 & 0 \\ 0 & \dfrac{-2(\pi-2\Phi_1)\cdot V_{34}}{\rm con\,1} & 0 \\ 0 & \dfrac{2(\pi-2\Phi_1)\cdot 2V_{\rm in}}{\rm con\,3} & \dfrac{-2}{C_t} \end{bmatrix} \begin{bmatrix} \tilde{v}_{\rm in} \\ \tilde{\phi}_1 \\ \tilde{i}_o \end{bmatrix} \\ \tilde{v}_o = [0\ \ 0\ \ 1][\tilde{i}_1\ \ \tilde{v}_{12}\ \ \tilde{v}_{34}]^T \end{cases} \tag{13}$$

where $\rm con\,1 = C_p T_s \omega \cdot 2\omega L_s$, $\rm con\,3 = C_t T_s \omega \cdot 2\omega L_s$, $C_t = C_s + 2C_o$.

2) *Small-Signal Characteristics of Open-Loop Converter in Boost Mode*: Equation (13) can also be expressed as

$$\dot{\tilde{x}} = A\tilde{x} + B\tilde{u}$$

$$y = C\tilde{x}$$

$$A = \begin{bmatrix} 0 & -\dfrac{1}{2L_{\rm dc}} & 0 \\ \dfrac{1}{C_p} & 0 & \dfrac{-2\Phi_1(\pi-\Phi_1)}{\rm con\,1} \\ 0 & \dfrac{2\Phi_1(\pi-\Phi_1)}{\rm con\,3} & \dfrac{-2}{C_t R} \end{bmatrix}$$

$$B = \begin{bmatrix} \dfrac{1}{Ldc} & 0 & 0 \\ 0 & \dfrac{-2(\pi-2\Phi_1)\cdot V_{34}}{\rm con\,1} & 0 \\ 0 & \dfrac{2(\pi-2\Phi_1)\cdot 2V_{\rm in}}{\rm con\,3} & \dfrac{-2}{C_t} \end{bmatrix}$$

$$C = [0\ \ 0\ \ 1].$$

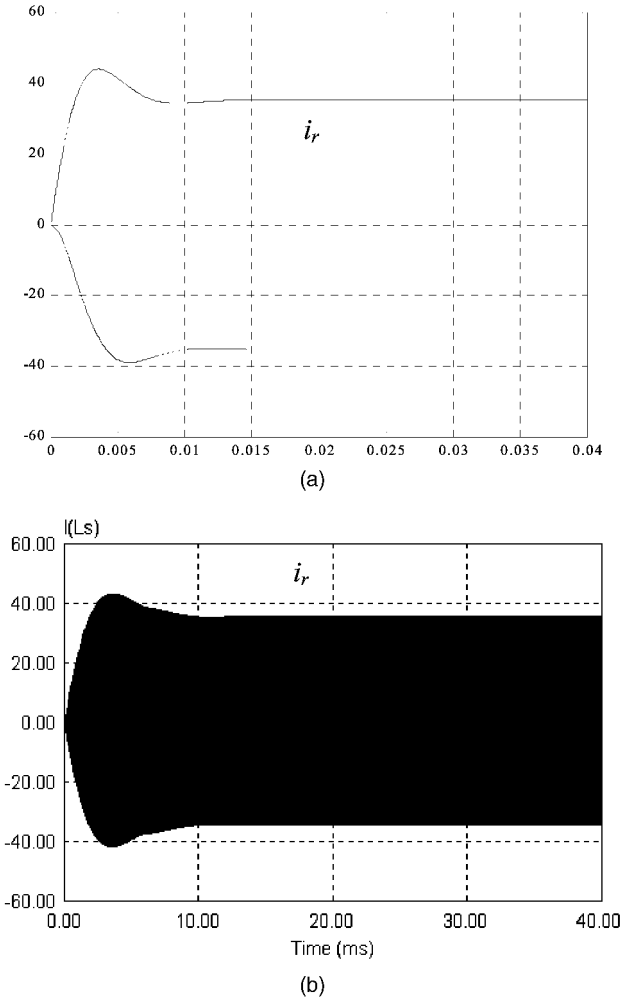

Fig. 12. Simulation and comparison of envelope of i_r in buck mode. (a) Envelope of i_r of average mode simulation. (b) Envelope of i_r of detailed circuit simulation.

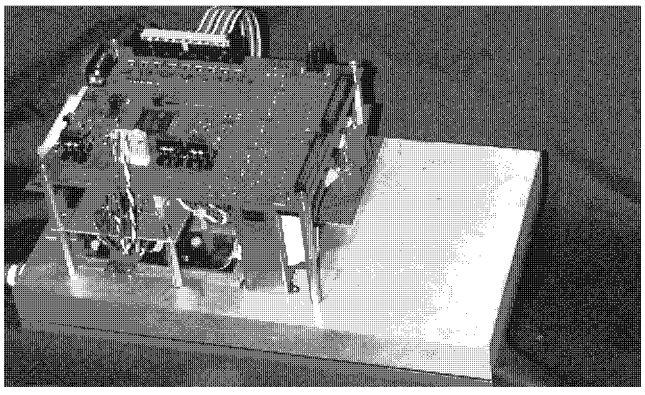

Fig. 13. Photo of prototype.

The transfer function matrix from input vector $\tilde{u}$ to output $\tilde{y}$ can be obtained

$$\begin{aligned}\tilde{v}_o(s) &= C(sI-A)^{-1}B\tilde{u}(s)\\ &= T_1(s)\tilde{v}_{\text{in}}(s) + T_2(s)\tilde{\phi}_1(s) + T_3(s)\tilde{i}_o(s). \end{aligned} \quad (14)$$

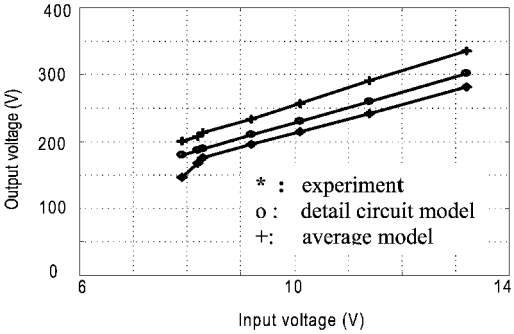

Fig. 14. Output characteristics comparisons.

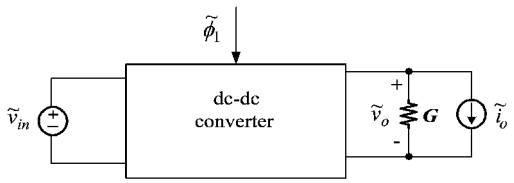

Fig. 15. Linearized small signal model.

The circuit parameter values used to derive the transfer functions are:

$$P_o = 1.6\text{ kW}, \quad V_{\text{in}} = 12\text{ V}, \quad \Phi_1 = 0.16\pi$$
$$R = 0.36\ \Omega, \quad L_{\text{dc}} = 5\ \mu\text{H}, \quad L_s = 0.30\ \mu\text{H}$$
$$C_p = C_s = 10\text{ mF}, \quad C_o = 169\text{ mF}, \quad f_s = 20\text{ kHz}.$$

$T_1(s)$, $T_2(s)$ and $T_3(s)$ can be calculated based on (14) as follows

$$\begin{aligned} T_1(s) &= \frac{\tilde{v}_o(s)}{\tilde{v}_{\text{in}}(s)} \\ &= \frac{0.31928480\times 10^9}{s^3 + 15.964s^2 + 0.10008869\times 10^8 s + 0.159642401\times 10^9} \\ T_2(s) &= \frac{\tilde{v}_o(s)}{\tilde{\phi}_1(s)} \\ &= \frac{617.048s^2 - 0.342804\times 10^6 s + 0.6170484580\times 10^{10}}{s^3 + 15.964s^2 + 0.10008869\times 10^8 s + 0.159642401\times 10^9} \\ T_3(s) &= \frac{\tilde{v}_o(s)}{\tilde{i}_o(s)} \\ &= \frac{-15.964s^2 - 0.159642401\times 10^9}{s^3 + 15.964s^2 + 0.10008869\times 10^8 s + 0.159642401\times 10^9}. \end{aligned} \quad (15)$$

The control-to-output transfer function $T_2(s)$ is the most important transfer function to study the dynamics and design the controller to allow the converter to meet load regulation and transient response specifications in boost mode. The root locus plot of $T_2(s)$ is shown in Fig. 16. The zeros and poles are as follows: $z1 = 277.8 + 3150.1i$, $z2 = 277.8 - 3150.1i$, $p1 = -15.95$, $p2 = -0.007 + 3163.7i$, $p3 = -0.007 - 3163.7i$.

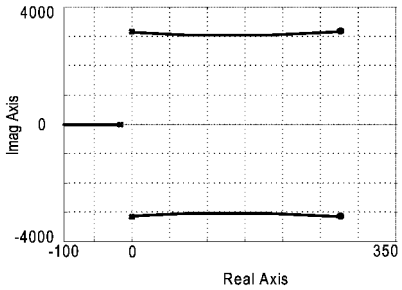

Fig. 16. Root locus plot of $T_2(s)$.

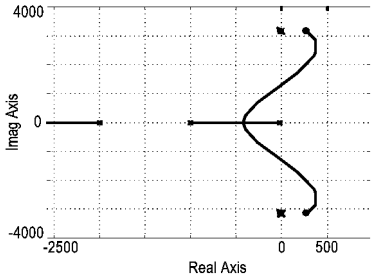

Fig. 17. Root locus of compensated system.

The transfer function has two zeros in the RHP and two poles very close to the $j\omega$-axis.

The distinct feature of small-signal dynamics of boost-type converter is the RHP zero. For DHB converter when the power flows from LVS to HVS, it is in fact a high-order boost converter. Therefore it repeats the inherent characteristics of boost converter. From the root locus of $T_2(s)$, the open-loop converter does not have much stability margin for the two poles very close to $j\omega$-axis. However, this is not a big concern because the model is derived based on the assumption that each device is ideal and no loss is taken into account. In fact, all the lossy components will add more inertia to the system so the converter is actually more stable than it is shown in Fig. 16. In addition, a good controller will add more stability margin.

3) *Closed-Loop System Analysis*: Based on the derived small-signal transfer functions of (15), a

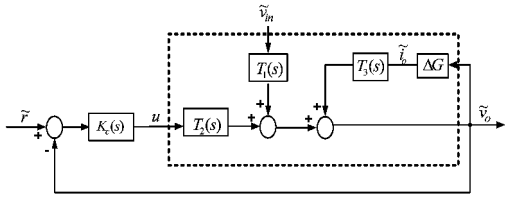

Fig. 18. Closed-loop model of small signal control system.

controller is designed to stabilize the system and to reduce the effect of exogenous disturbances on the system. The controller is obtained as

$$K_c(s) = \frac{K(s + 0.008 + 3160i)(s + 0.008 - 3160i)}{(s + 1000)(s + 2000)}.$$

The root locus of the compensated system is shown in Fig. 17.

The two zeros of the controller cancel the effect of two nearly pure imaginary poles of the uncompensated system. The two poles of the controller ensure that the root locus does not go into the right plane with a small gain, thus making the system more stable. The transient response mainly depends on the pair of poles. If K is selected as 0.44, the poles are calculated as follows: $p1 = -160 + 947.5112i$, $p2 = -160 - 947.5112i$.

The block diagram of the control system is shown schematically in Fig. 18. To estimate the system performance, a simulation model of close-loop control system is established in Fig. 19. The simulation results are shown in Figs. 20–22, in which v_{34} is the primary-referred output voltage. The circuit parameters of simulation model are defined earlier in the paper. Fig. 20 plots the system performance when the load changes from 0.36 ohm to 0.4 ohm at $t = 0.1$ s. The reference input voltage is 24 V. The input current i_1 decreases because less power is required at lighter load if the same output voltage is required. v_{12}, the voltage across $C1$ and $C2$, is unchanged because it depends on the battery voltage v_{in}, which equals to 12 V and does not change in this case. The overshoot of output voltage v_{34} is less than 0.2%. Fig. 21 shows the output performance when

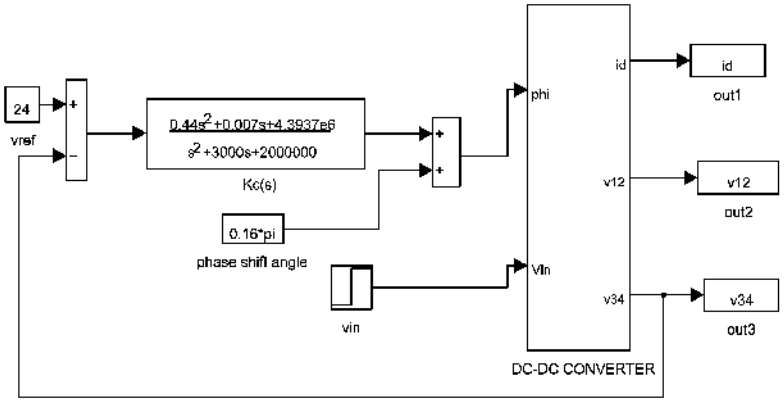

Fig. 19. Simulation model of small signal control system.

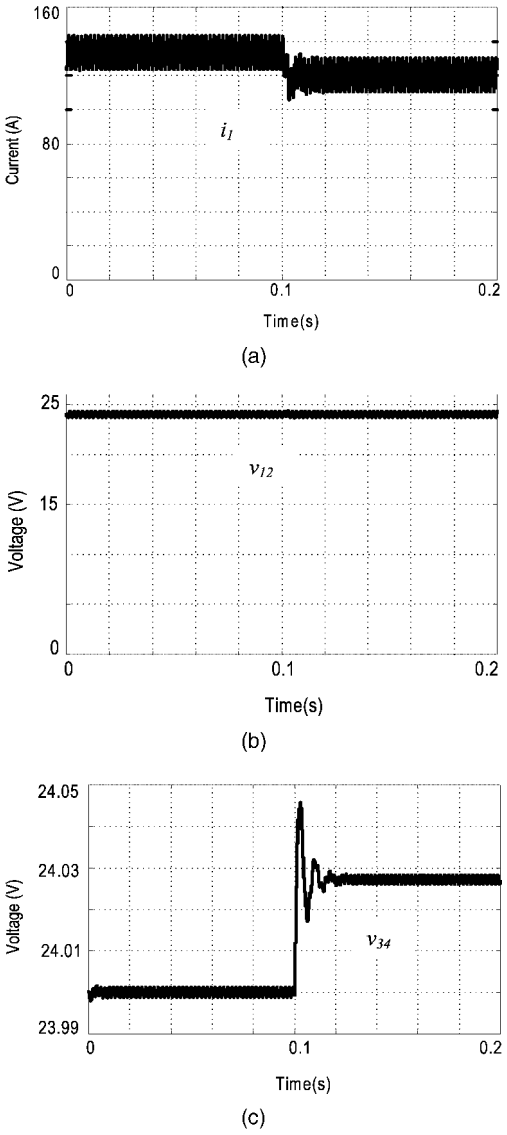

Fig. 20. System response of load step change from 0.36 Ω to 0.4 Ω. (a) i_1 response of load step change (from 0.36 Ω to 0.4 Ω). (b) v_{12} response of load step change (from 0.36 Ω to 0.4 Ω). (c) v_{34} response of load step change (from 0.36 Ω to 0.4 Ω).

the battery voltage v_{in} changes from 12 V to 11 V and the reference voltage remains at 24 V with the load unchanged. v_{12} decreases from 24 V to 22 V (which is not shown in the figure), and v_{34} drops less than 0.03 V. Fig. 22 shows the dynamic response to a change in the reference voltage. When the reference voltage changes from 24 V to 25 V, the output voltage follows the reference command in a short time with a small overshoot.

The simulation results show that the designed controller provides a satisfactory transient response for fuel cell systems. However, the designed controller is not the optimum one in terms of robustness. Other advanced control algorithms can be applied to this converter easily with the derived small signal model and is beyond the scope of this work.

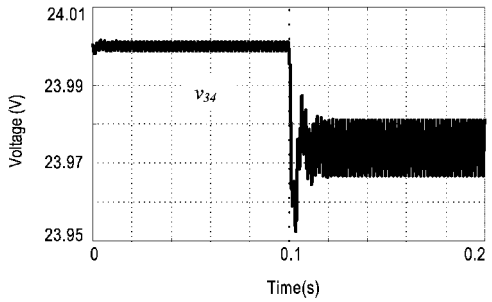

Fig. 21. Output response of input voltage step change from 12 V to 11 V.

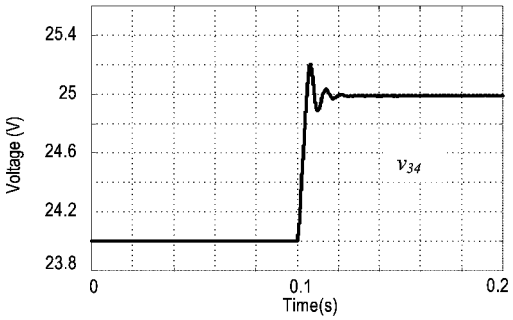

Fig. 22. Output response when reference voltage step changes from 24 V to 25 V.

V. CONCLUSION

This paper is concentrated on developing a unified state-space mathematical model in both boost mode and buck mode for a new DHB bidirectional dc-dc converter. The steady-state characteristics and dynamic behavior of the converter in boost mode have been derived based on the model. Those analyses of buck mode can be derived similarly. The steady-state characteristics derived from the mathematical model are consistent with the one derived from circuit analysis. It is also shown in this paper that DHB converter of boost mode has RHP zeros and therefore repeats the small signal dynamics of the boost type converter. The mathematical model provides a fast simulation tool to study the start-up performance, stability and the transient response of the proposed converter against load variation and changed battery voltage. The optimum controller can be thereby designed based on the derived small signal model for both modes, which the authors are currently working on.

REFERENCES

[1] Wang, K., et al. (1998)
Bi-directional dc to dc converters for fuel cell systems.
In *Conference Record of 1998 IEEE Workshop on Power Electronics In Transportation*, 47–51.

[2] Wang, K., et al. (2000)
Design, implementation, and experimental results of bi-directional full-bridge DC/DC converter with unified soft-switching scheme and soft-starting capability.
In *Conference Record of 2000 IEEE Power Electronics Specialist Conference*, 1058–1063

[3] Reimann, T., Szeponik, S., Berger, G., and Petzoldt, J. (1997)
A novel control principle of bi-directional dc/dc power conversion.
In *Conference Record of 1997 IEEE Power Electronics Specialist Conference*, 978–984.

[4] De Donker, R. W., Divan, D. M., and Kheraluwala, M. H. (1991)
A three-phase soft-switched high power density dc/dc converter for high power applications.
IEEE Transactions on Industry Applications, (Jan./Feb. 1991), 63–73.

[5] Li, H., Peng, F. Z., and Lawler, J. (2001)
A natural ZVS high power bi-directional dc-dc converter with minimum number of devices.
In *Conference Record of IAS*, 2001, 1874–1881.

[6] Li, H., Peng, F. Z., and Lawler, J. (2001)
Modeling, simulation, and experimental verification of soft-switched bi-directional dc-dc converters.
In *Conference Record of APEC*, 2001, 736–742.

[7] Sun, J., and Grotstollen, H. (1992)
Averaged modeling of switching power converters: Reformulation and theoretical basis.
In *IEEE PESC Record*, 1992, 1162–1172.

[8] Lin, J., and Hsieh, H. Y. (2000)
Dynamics analysis and controller synthesis for zero-voltage-transition PWM power converters.
IEEE Transactions on Power Electronics, **15**, 2 (Mar. 2000), 205–214.

[9] Ioinovici, A. (1988)
Transient analysis of DC to DC converters in discontinuous operation mode by using alternator equations.
IEEE International Symposium on Circuits and Systems, 1988, 1381–1384.

[10] Ioinovici, A. (1990)
Simulation of quasi-resonant converters in half-wave mode operation mode by using modified equations.
IEEE international Symposium on Circuits and Systems, 1990, 665–668.

[11] Erickson and Maksimovic (2000)
Fundamentals of Power Electronics (2nd ed.), Boston: Kluwer Academic Publishers, 2000.

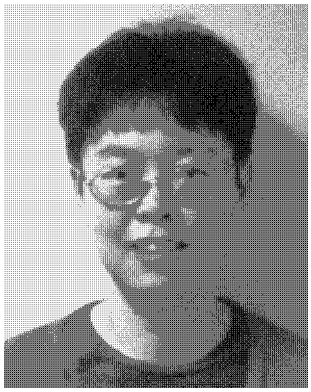

Hui Li (S'97—M'00—SM'01) received the B.S. and M.S. degree in electrical engineering from Huazhong University of Science & Technology, China in 1992 and 1995, respectively. She received the Ph.D. degree in electrical engineering from the University of Tennessee, Knoxville in 2000. From 1999 to 2000, she worked for Power Electronics and Electric Machinery Research Center of Oak Ridge National Laboratory on developing soft-switching power converter for hybrid electric vehicle, uninterrupted power supply and motor drive application. In 2001, she joined Tyco Electronics working on high efficiency high power density rectifier and dc-dc converter. Currently she is an assistant professor of Electrical and Computer Engineering Department, Florida State University.

Her research interests include soft-switching converters, motor drive control, modeling and simulation of power electronics system, application of new power semiconductor devices. She is an IEEE senior member.

Fang Zheng Peng (M'92—SM'96) received the B.S. degree in electrical engineering from Wuhan University, China, in 1983 and the M.S. and Ph.D. degrees in electrical engineering from Nagaoka University of Technology, Japan, in 1987 and 1990, respectively.

He joined Toyo Electric Manufacturing Company, Ltd., from 1990 to 1992 as a research scientist, was engaged in research and development of active power filters, flexible ac transmission systems (FACTS) applications and motor drives. From 1992 to 1994, he worked with Tokyo Institute of Technology as a research assistant professor, initiated a multilevel inverter program for FACTS applications and a speed-sensorless vector control project. From 1994 to 2000, he worked for Oak Ridge National Laboratory (ORNL), as a research assistant professor at University of Tennessee, Knoxville from 1994 to 1997 and was a staff member, lead (principal) scientist of the Power Electronics and Electric Machinery Research Center at ORNL from 1997 to 2000. Since 2000, he joined Michigan State University as an associate professor of the Department of Electrical and Computer Engineering.

Dr. Peng received many awards including the 1996 First Prize Paper Award and the 1995 Second Prize Paper Award of Industrial Power Converter Committee in IEEE1/IAS2 Annual Meeting; the 1996 Advanced Technology Award of the Inventors Clubs of America, Inc., the International Hall of Fame; the 1991 First Prize Paper Award in IEEE Transactions on Industry Applications; and the 1990 Best Paper Award in the Transactions of the IEE3 of Japan, the Promotion Award of Electrical Academy. He has been an associate editor for IEEE Power Electronics Transactions since 1997 and chair of technical committee for Rectifiers and Inverters of IEEE Power Electronics Society. Dr. Peng holds 10 patents.